SAMPLE-BASED ROBUST UNCERTAINTY PROPAGATION FOR ENTRY VEHICLES

Remy Derollez[*] **Zachary Manchester**[*]

This paper introduces a new approach for uncertainty quantification and propagation applicable to entry vehicle trajectories, suitable for use in trajectory optimization and computation of approximate invariant funnels. Because of the lack of precise knowledge of the atmospheres of other solar system bodies, traditional entry trajectory design methods rely on extensive Monte Carlo simulations, leading to accurate results but at high labor and computational costs. Other conventional methods can be faster but require assumptions on the probability distributions of dispersion parameters. The approach developed in this paper represents uncertainties in the system using conservative ellipsoidal bounds. A sample-based strategy inspired by the Unscented Kalman Filter is used to propagate the dynamics and uncertainties around the nominal trajectory. The method is demonstrated on the Duffing oscillator and then applied to a Mars entry vehicle problem using both three-degree-of-freedom and six-degree-of-freedom dynamical models. Its performance is compared with traditional uncertainty quantification methods.

INTRODUCTION

The future ambitions of multiple space agencies, including NASA, target the Moon and Mars as future destinations. The Entry Descent and Landing (EDL) phase is a crucial part of all these missions that require landing on another celestial body. Knowledge of a planet's atmospheric parameters, winds, and the position and velocity of the entry vehicle are all imperfect. Therefore, managing uncertainty is a fundamental problem in entry guidance and is critical to achieving the objectives of the planned missions while meeting safety and accuracy requirements.

New NASA missions seek to land larger payloads with increased precision on Mars, for example, to achieve proximity with pre-positioned robotic assets. As mentioned in the literature,[1] most of the processes used today still heavily rely on methods developed for the Viking missions in the 70's.[2] Most of the uncertainty analysis is performed using Monte Carlo methods[3–5] which are time-consuming and computationally heavy. In contrast, Polynomial Chaos Expansion (PCE) has been applied to hypersonic flight dynamics as shown by the work of Prabhakar and al[6] but PCE does not scale well with the dimension of the uncertainty space. More recently, Jin and al. applied linear covariance (linCov) techniques to the entry problem on a three-degree-of-freedom model and compared the results to a Monte Carlo analysis.[7] Woffinden and al. went further to apply similar linear covariance analysis techniques to atmospheric flight during EDL phase but this time on a full six-degree-of-freedom dynamical model to generate navigation systems requirements for the Safe and Precise Landing – Integrated Capabilities Evolution (SPLICE) project.[8] While these new approaches are usually faster than traditional Monte Carlo analyses, some require assumptions on the probability distributions followed by the parameters analyzed which is difficult to infer given the

---

[*]Department of Aeronautics and Astronautics, Stanford University, 496 Lomita Mall, Stanford, CA 94305.

relatively small amount of data available on Mars environment. Others are rather destined to dispersion analysis for system design and would be difficult to integrate in an optimization framework.

This paper presents a method that does not assume any prior knowledge on the type of distribution followed by the uncertain variables and therefore provide conservative bounds on the trajectory taken by the vehicle. In order to obtain guarantees on the safety and performance of the real trajectory, we only use bounds on the uncertain parameters based on data obtained on the Mars environment. The introduction and the propagation of these bounds through the non-linear dynamics allows us to propagate uncertainties in a more accurate way than linearization techniques and at a relatively low computational cost compared to traditional Monte Carlo dispersion analyses. The approach developed also scales way better than Polynomial Chaos Expansion techniques. Our work is applicable to a full six-degree-of-freedom non-linear dynamic entry model with no dimension reduction and can be easily incorporated in trajectory optimization solvers. In this work, we primarily focus on the EDL phase of a low lift-to-drag ratio vehicle on a Mars mission.

This paper proceeds as follows: The first section provides the necessary background related to uncertainty propagation techniques as well as sum-of-squares programming and previous work on robust funnel computation. We then present our sample-based approach principles and detail its application on the example of the Duffing oscillator. The aforementioned technique is applied to the entry vehicle problem on the traditional three-degree-of-freedom (3 DOF) Vinh's model as well as on a full six-degree-of-freedom (6 DOF) entry model. Our method's performance is analyzed and compared with Monte Carlo, Linear Covariance Analysis and Polynomial Chaos Expansion techniques.

BACKGROUND

In this first section we give some elements on uncertainty quantification methods used in this paper. In particular we give the basis of two probabilistic methods: linear covariance analysis techniques and polynomial chaos expansions. The work of Luo and Yang give a general overview of uncertainty approaches used in astrodynamics.[9]

Linear Covariance Analysis

When considering a random vector x following a given distribution, one way to propagate uncertainties is simply to linearize the system dynamics $f(x, t)$ around the nominal unperturbed trajectory using a first-order Taylor expansion. If we define, $m(t)$ as the mean of the random variable x at time t and $\Sigma(t)$ its covariance matrix, we have the following well known formulae,

$$m(t) = \Phi(t, t_0)m(t_0), \tag{1}$$

$$\Sigma(t) = \Phi(t, t_0)\Sigma(t_0)\Phi(t, t_0) + Q, \tag{2}$$

where $\Phi(t, t_0) = \exp A(t - t_0)$ is the state transition matrix (STM) computed using the matrix $A = \frac{d}{dt}f(x, t)|_{x=x_{nom}}$, giving the first order approximation of the dynamics around the nominal trajectory. These equations form the basis of linear covariance analysis techniques enabling to propagate the mean and the covariance of the random vector further in time, with the assumption of random noise of covariance matrix Q added to the dynamics. More detailed information on this

approach can be found in the work of Maybeck.[10] Note that the equations derived above are the continuous version of the formulae used in the prediction step of the Extended Kalman Filter (EKF).

Polynomial Chaos Expansion

Polynomial Chaos Expansion (PCE) enables to approximate the solution of a stochastic differential equation (differential equation with uncertain parameters) that is square-measurable, possibly non-Gaussian, with respect to the input uncertainties. In this sense it is the stochastic pendant of Sturm-Liouville theory and the associated generalized Fourier decomposition used for deterministic partial differential equations. Unlike traditional methods, PCE involves a non-linear propagation of the system's state and is not restricted to Gaussian random inputs. The approximation of the solution u of a stochastic equation (depending on one random parameter ξ) using PCE is the best linear approximation of the true solution in the sense that,

$$\mathbb{E}[u(t,.) - u_p(t,.)] \ \rightarrow \ 0, \ \ p \rightarrow \infty, \tag{3}$$

where p is the order of the polynomial approximation and the convergence is mean square. We can therefore write the approximation of the solution as a linear combination of a given family of polynomial $(\phi_i)_{i=0}^p$ which depends on the type of distribution followed by the uncertainty parameter ξ,

$$u_p(t,\xi) = \sum_{i=0}^p c_i(t)\phi_i(\xi). \tag{4}$$

Therefore our solution is entirely determined by the vector of coefficients $(c_i)_i$. Interestingly, the moments of the probability distribution characterizing the state uncertainty of the system at time t are directly related to the values of the coefficients at that time. In this paper, we use a non intrusive method[11] for determining the coefficients. It makes use of the full non-linear dynamics and relies on a sampling method which involves solving a relatively simple least-square regression problem on the sampled data at each time step. The reader can find a complete treatment of PCE and associated methods in the work of Xiu.[12]

Sum-Of-Squares Programming

At the core of our approach to entry guidance are sum-of-squares (SOS) verification techniques. SOS methods have been developed in the robotics community over the past decade to enable control of complex mechanical systems with guarantees on safety, robustness, and performance in the presence of disturbances and uncertainty. A polynomial is said to be a sum-of-squares if it can be written as a sum of squared terms. The immediate consequence is the non-negativity of the polynomial on the domain of interest. Given any polynomial P, we can write $P = z^T C z$, where the vector z contains all the monomials up to a given degree and C is a matrix of coefficients. It turns out that if the matrix C is positive definite, then the corresponding polynomial P is SOS, therefore making the link between SOS and Semi-Definite Programming (SDP). It follows that SOS methods can be used to find polynomial Lyapunov functions and, consequently, to the study of stability of complex dynamical systems. Given a dynamical system, stability of the origin can be proven if a non-negative scalar function

$$V(x) \geq 0, \tag{5}$$

can be found that decreases along trajectories of the system:

$$\dot{V} = \nabla V \cdot f(x, u, w) \leq 0. \tag{6}$$

Robust Invariant Funnels and DIRTREL

The basic sum-of-squares technique outlined above can be extended in many ways. In particular, it can be used to find *invariant funnels*, which are time-varying versions of basins of attraction. Loosely, an invariant funnel can be thought of as a tube around a reference trajectory within which a tracking controller is guaranteed to stabilize the system (Figure 1). Funnels have attracted widespread interest in the robotic motion planning community in recent years and have been used to solve a variety of challenging control problems.
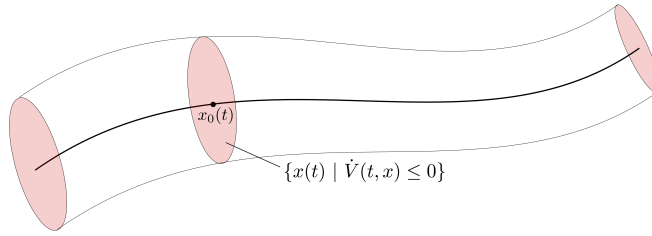
Figure 1. Conceptual depiction of an invariant funnel around a reference trajectory.

In addition to certifying the stability of tracking controllers under nominal conditions, robust invariant funnels can be computed that account for bounded disturbances. In this context, they can provide error ellipsoids along a nominal trajectory without resorting to Monte Carlo simulation. This approach is used in the DIRTREL (DIRect TRanscription with Ellipsoidal disturbances and Linear feedback) algorithm developed by Manchester and Kuindersma,[13] which provides a robust trajectory optimization framework by using approximate invariant funnels. Disturbances are assumed to be contained in an ellipsoidal set and the uncertainty on the state is represented as an ellipsoidal region at each time step as well. By linearizing the dynamics, the authors are able to derive a closed form equation providing the evolution of the state uncertainty region given some initial bounds on the state and some bounds on the perturbation parameters.

The essence of the present paper is to extend the uncertainty propagation technique of DIRTREL by using the full non-linear dynamics and computing approximate invariant funnels using a sampling method. Just as the Unscented Transform used in the UKF provides a sample-based analog of linear covariance analysis, we develop a sampled-based version of the DIRTREL algorithm for entry vehicle applications. However, the reader should remember that, unlike the methods mentioned above, SOS methods are mathematical verification methods inherently concerned with obtaining robust guarantees on the trajectory of the system and, therefore, focus on finding conservative bounds on the trajectory. There is therefore a difference in nature between the bounds obtained through these verification techniques and the statistical limits that are given by methods like linear covariance analysis, Monte Carlo simulations, or polynomial chaos expansions, making the distinction between probabilistic methods on the one hand and bounded set propagation methods like DIRTREL and the one developed in this paper on the other hand.

SAMPLE-BASED UNCERTAINTY PROPAGATION

Uncertainty Representation

We first assume that the discrete-time dynamics function of our system is given by

$$x_{i+1} = f(x_i, u_i, w_i), \tag{7}$$

where x_i represents the state vector of the system at time step i, u_i is the control input on the system and w_i represents a vector of disturbances acting on the system at time i that can be related to unmodeled dynamical effects, noise, or state estimation errors. Note that we do not restrict the perturbation w_i to be additive. Next we define the uncertainty regions as ellipsoidal sets. The disturbance values are constrained to belong to the set

$$D_i = \{w \mid w^T S_i^{-1} w \leq 1\}, \tag{8}$$

and the state vector uncertainty region is modeled as the ellipsoid centered in $\bar{x}_i$ and parameterized by E_i,

$$U_i = U(\bar{x}_i, E_i) = \{x \in \mathbb{R}^n \mid (x - \bar{x}_i)^T E_i^{-1}(x - \bar{x}_i) \leq 1\}, \tag{9}$$

where S_i and E_i are positive definite matrices and n is the dimension of the space in which the ellipsoids are computed, most of the time equal to the dimension of the state space of the dynamical model in use.

Uncertainty Propagation

Given an uncertainty region at time step i, we want to propagate this region according to the dynamics of our system to obtain conservative uncertainty bounds at the following time step $i + 1$. Linearizing the dynamics would allow us to propagate the ellipsoidal uncertainty regions in a closed form as the image of an ellipsoidal set by a linear function remains an ellipsoidal set. However, in this paper we extend the approach developed in DIRTREL by using a sampling method and make use of the full non-linear dynamics of the system. In this sense, instead of working with the information contained in the linear form of the dynamics, we use the full dynamics but access the information by selecting a certain number of points to be propagated.

We extract some points in the uncertain region at time i according to a chosen sampling scheme. We denote the sampled points at time i as $(x_i^k)_{k=1,\ldots,m}$. These points are then propagated using the dynamics to obtain the points $(\hat{x}_{i+1}^k)_{k=1,\ldots,m}$ satisfying

$$\hat{x}_{i+1}^k = f(x_i^k, u_i, w_i), \quad k = 1, \ldots, m. \tag{10}$$

Note the difference between the points $(\hat{x}_{i+1}^k)_{k=1,\ldots,m}$ obtained after propagation of the sampled points at time step i, $(x_i^k)_{k=1,\ldots,m}$ and the set of points $(x_{i+1}^k)_{k=1,\ldots,m}$, characterizing the sampled points at time step $i+1$. We solve a convex optimization problem to fit a minimum-volume enclosing ellipsoid (MVEE) enclosing the propagated points to obtain our uncertainty region characterized by the matrix E_{i+1} at step $i + 1$. The points $(x_{i+1}^k)_{k=1,\ldots,m}$ are sampled using the obtained ellipsoid E_{i+1}.

$$E_{i+1} = \text{MVEE}[(\hat{x}_{i+1}^k)_k \mid \hat{x}_{i+1}^k = f(x_i^k, u_i, w_i), x_i^k \in U_i, w_i \in D, k = 1, \ldots, m]. \qquad (11)$$

The MVEE fitting algorithm is detailed in the next section. Figure 2 provides a schematic of the corresponding process in the case $n = 2$ and Algorithm 1 represents the sample-based procedure in a more general and rigorous way.
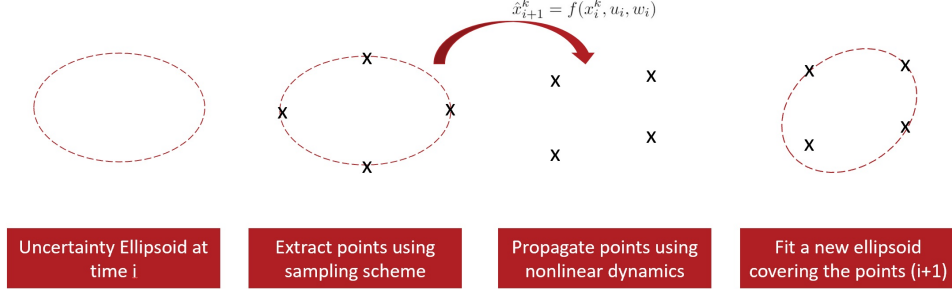
Figure 2. Uncertainty propagation principle in 2D

Algorithm 1: Ellipsoidal uncertainty regions propagation algorithm

Input : Initial ellipsoidal uncertainty region, A_0, b_0, D

1 **procedure**
2 $A \leftarrow A_0$;
3 $b \leftarrow b_0$;
4 **for** $i = 1$ *to* N **do**
5 $\quad (x_i^k)_{k=1,\ldots,m} \leftarrow \textbf{EXTRACT}(A_i, \ b_i)$;
6 $\quad (\hat{x}_{i+1}^k)_{k=1,\ldots,m} \leftarrow \textbf{PROPAGATE}((x_i^k)_{k=1,\ldots,m}, u_i, w_i)$;
7 $\quad A_{i+1}, \ b_{i+1} \leftarrow \textbf{MVEE}((\hat{x}_{i+1}^k)_{k=1,\ldots,m})$;
8 **end**
9 **return** $(A_i, \ b_i)_i$
10 **end procedure**

The reader will note the resemblance with the dynamic propagation step of the Unscented Kalman Filter (UKF). While linearization techniques usually approximate the dynamics of the system locally and propagate Gaussian disturbances through it (analog to the Extended Kalman Filter), the unscented filter still makes use of the full non-linear dynamics of the system and selects and propagates only special points (exhibiting the same statistical properties as the corresponding distribution) enabling an accurate reconstruction of the distribution after propagation. The difference with our approach lies in its conservative nature, as the bounds that we use do not correspond to a statistical confidence level and do not assume an underlying probability distribution.

Note that, in the majority of the applications treated in this paper, the sampling scheme corresponds to the semi-major axes of the ellipsoid at each time in both directions and of the geometric center of the ellipsoid ($2n + 1$ points). This is similar to the sigma point selection heuristic in the unscented transform procedure, which enables to approximate the first two moments of the distribution up to first and second order respectively. Once again however, instead of selecting points on the sublevel set of a probability function, our points lie exactly on the boundary of the conservative

uncertainty ellipsoid. Just like the UKF procedure can be extended to propagate and recover more information,[14] a more elaborate sampling scheme can allow us to propagate conservative bounds on the dynamics for a system containing higher order non-linearities. The amount of information accessed and propagated is directly related to the sampling scheme.
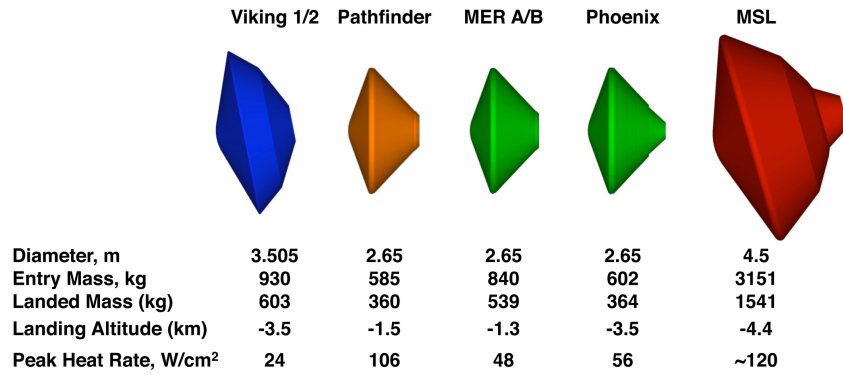
Ellipsoid Fitting Process

We now detail the fitting procedure as performed by the **MVEE** function used in Algorithm 1. For any time step i we define the symmetric matrix A_i satisfying $A_i^2 = E_i^{-1}$. A_i is a square root of E_i^{-1} and the columns of $A_i^{-1} = E_i^{\frac{1}{2}}$ give the directions characterizing the semi axes of the ellipsoidal region and are therefore directly related to the uncertainty in the associated direction. In this section we represent the ellipsoidal uncertainty set with the matrix $A_i \in \mathbb{R}^{n \times n}$ and the vector $b_i \in \mathbb{R}^n$. This choice is simply for convenience when formulating the fitting problem as stated below. We can relate our different representations using $E_i = A_i^{-2}$ and $\bar{x}_i = -A_i^{-1} b_i$. Given a set of propagated points at time $i + 1$, the objective is to find the ellipsoid in dimension n, parameterized by the matrices A and b that covers the set of points while minimizing its volume. The volume of a given ellipsoid is inversely proportional to the determinant of the matrix A and this classical optimization problem can be reformulated as[15]

$$
\begin{array}{ll}
\underset{A,b}{\text{minimize}} & -\log \det (A) \\
\text{s.t.} & ||A\hat{x}_{i+1}^k + b|| \leq 1 \; k = 1, \ldots, m.
\end{array}
\tag{12}
$$

Note that the time step subscript $i + 1$ has been dropped for convenience, but it should not be forgotten that a convex optimization problem is solved at each time step. In this work, we first resorted to the use of Mosek.[16] This commercial solver gives good performance but can run into some difficulty when dealing with some edge cases. In practice, the optimization process can run into numerical issues linked to the range and the scaling of the points. Similarly, as the dimension of the space increases, numerical errors associated with finite-precision arithmetic can grow. In order to overcome these difficulties and to improve the performance of the process, a custom solver for this problem was implemented. It is inspired by the Dual Reduced Newton algorithm developed by Freud et al[17] with some changes mainly in the line search procedure.

ENTRY VEHICLE MODELS

This section briefly details the entry dynamics models used in this paper for the application of the sample-based uncertainty propagation method. We consider a sphere-cone forebody entry vehicle geometry, as it has been used previously for the Viking, Pathfinder, Phoenix,[18] Mars Exploration Rover (MER) and Mars Science Laboratory (MSL) missions. It is indeed the optimized geometry providing a low ballistic coefficient which is required to accomplish relevant deceleration during entry but also enabling to keep the temperature relatively low. Note that in considering future crewed missions to Mars, for which the mass is predicted to be around 20 metric tons (or about 20 times the mass of MSL), the geometry of the interplanetary vehicle might be different.[19] However, our code uses a panel method to compute the aerodynamic coefficients and is therefore flexible on the geometry considered. Figure 3 shows the geometry of previous missions.

	Viking 1/2	Pathfinder	MER A/B	Phoenix	MSL
Diameter, m	3.505	2.65	2.65	2.65	4.5
Entry Mass, kg	930	585	840	602	3151
Landed Mass (kg)	603	360	539	364	1541
Landing Altitude (km)	-3.5	-1.5	-1.3	-3.5	-4.4
Peak Heat Rate, W/cm^2	24	106	48	56	~120

Figure 3. Previous NASA Mars missions geometry

The aerodynamics is a major component of the entry dynamics as the interaction of the vehicle with the atmosphere of the planet mainly determines the type of trajectory and its range. As traditionally used in hypersonic flight, we use Newton's impact theory to compute the aerodynamic coefficients as a function of the total angle of attack.[20] In brief, this theory considers that incoming flow molecules individually impact the vehicle surface element yielding the normal component of their linear momentum and retaining the parallel component of it. Simple formulae can be derived to obtain the local pressure coefficient and therefore the aerodynamic forces and moments by integration. The values of these coefficients are precomputed and stored in look-up tables.

Entry vehicle dynamics can suffer from instabilities as recalled in the work of Bibi and al.[21] For a more accurate modeling of the entry dynamics, we compute the dynamic derivatives with respect to the angular velocity components (which are the most important dynamic derivative terms). They allow us to take into account the damping phenomena due to the angular rotation of the vehicle and therefore provide a better stability of the vehicle when entering the atmosphere as detailed in the work of Gallais.[22]

The simulation of the Martian environment uses the data from MarsGRAM 2010. A Julia wrapper module has been implemented with the objective of incorporating and using the data easily in the trajectory simulation code enabling a reduction of computation expenses. Most of the data used in the following simulations correspond to a standard configuration (absence of extreme winds and absence of dust particles in the atmosphere). Note that these conditions can be easily modified to consider different scenarios in the future.

In both models the only control input considered is the bank angle. As we do not consider optimal control strategy so far, it is a defined sequence of values making the vehicle stable just as in the work of Benito and Mease.[23] The control input will be of bigger importance when performing trajectory optimization.

3 DOF Model

The three-degree-of-freedom model usually used in the domain of atmospheric entry does not take into account the full rotational motion of the capsule. The specific energy of the capsule is known at the start and at the end of the dynamics. Profiles are provided for the attack angle and the bank angle based on experimental data and requirements and are then adjusted to satisfy the constraints on drag, dynamic pressure and heat that the vehicle undergoes. The system of equations

describing the dynamics for this approach is known as the Vinh's model and can be found in the work from Manrique et al.[24] This representation uses the position vector of the center of mass of the vehicle in spherical coordinates and flight path and heading angles for the direction of the velocity vector.

6 DOF Model

The six-degree-of-freedom model takes into account rigorously both the translational and rotational motion of the capsule. As a consequence it is able to render the possibly unstable behavior of the capsule model phenomena more accurately, therefore being closer to the real dynamical behavior. This type of model is also interesting for modeling potential actuators in a more accurate way. Our approach uses quaternions to propagate the attitude of the vehicle and our state vector is written in a 13-dimensional space as

$$X = [x,\ y,\ z,\ q_0,\ q_1,\ q_2,\ q_3,\ \dot{x},\ \dot{y},\ \dot{z},\ \omega_x,\ \omega_y,\ \omega_z], \tag{13}$$

where we express the position and velocity of the spacecraft in the cartesian frame centered with the planet fixed. q_0 is the scalar part of the quaternion representing the attitude of the vehicle with respect to the inertial frame and ω_x, ω_y, ω_z are the components of the angular velocity vector of the vehicle in the body frame. The forces considered include gravity (with J2 effect) and aerodynamic forces (lift, drag, and aerodynamic moments).[25,26] Aerodynamic loads and moments are computed using the aerodynamic coefficients as detailed above. The full motion of the vehicle is given by the well known Newton-Euler system of equations and the associated kinematics equations (position vector and quaternions). The inertia parameters used for the simulation are shown in Table 1.

Table 1. 6 DOF nominal parameters

Parameter	Value
Mass [kg]	600.0
Inertia Matrix [kg.m^2]	$\begin{bmatrix} 160.0 & 0.0 & 40.0 \\ 0.0 & 160.0 & 0.0 \\ 40.0 & 0.0 & 200.0 \end{bmatrix}$
COM position [m]	[0.001, 0.0, -0.189]

Even if quaternions are an efficient and convenient way to propagate the attitude of the vehicle forward in time, there are not really adapted to uncertainty work. When needed in the following, the attitude of the vehicle is represented by the rotation vector (unconstrained attitude parameterization). The kinematics and dynamics equations linking the two representations can be found in the paper from Diebel.[27] Similarly when propagating ellipsoids in our sample-based method, we switch to this other representation. In addition, we use the trick implemented in the multiplicative extended Kalman Filter (MEKF) usually used for attitude errors propagation in aerospace. We therefore deal with the rotation vector characterizing the attitude error with respect to a reference.[28] At each time step, the reference is chosen to be the center of the ellipsoid for convenience and to reduce numerical errors.

RESULTS

The Duffing Oscillator

In this section, we apply our sample-based uncertainty approach to the Duffing oscillator. It allows us to validate our approach on a classic non-linear system that is easy to visualize. We recall the nonlinear second order differential equation characterizing the dynamics of the Duffing oscillator

$$\ddot{x} + \delta\dot{x} + \alpha x + \beta x^3 = \gamma\cos\omega t, \tag{14}$$

where $\dot{x}$ refers to the first derivative of the state variable with respect to the independent variable of time t. We summarize the values of the parameters used in the following simulation in Table 2. A feedback linear controller is added and additive Gaussian noise is implemented in the dynamics as well. Figures 4 to 6 show the trajectory of the center of the ellipses and compare it with the nominal trajectory both in position and in velocity. Figure 7 also shows the propagation of the ellipses for the first ten time steps giving some information on the dynamics behaviour for that time range. We also plot the dispersion around position and velocity and compare the results with Monte Carlo, linear covariance analysis and PCE methods as shown on Figures 8 and 9.
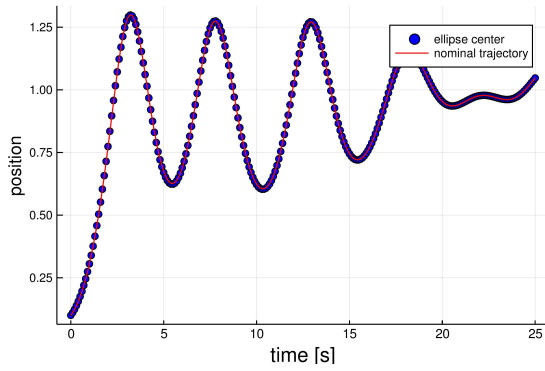
Figure 4. Position
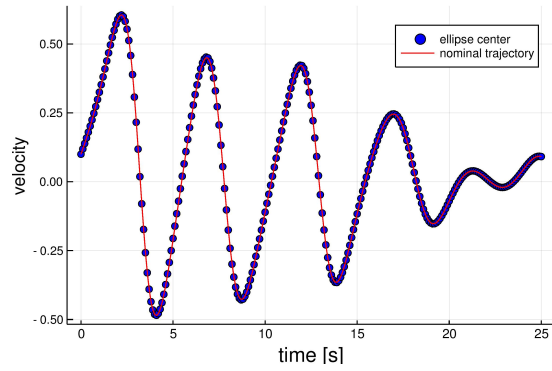
Figure 5. Velocity
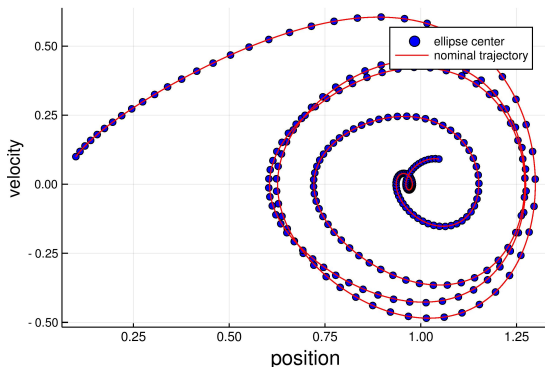
Figure 6. Phase portrait
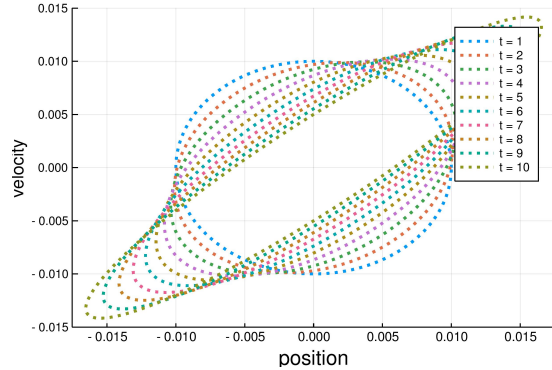
Figure 7. Ellipses propagation

10
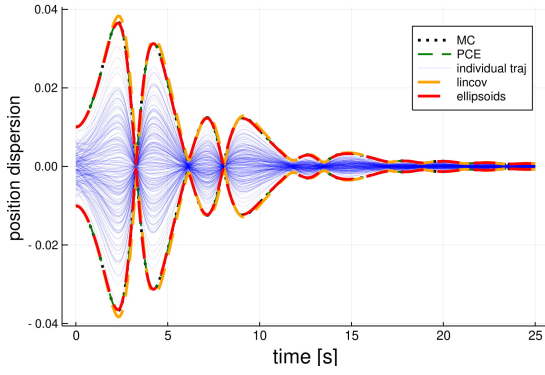
Figure 8. Position dispersion
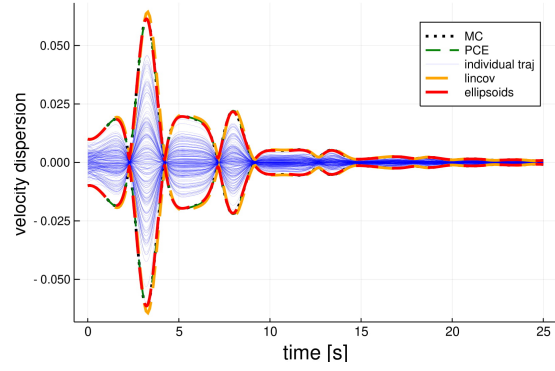
Figure 9. Velocity dispersion

Table 2. Duffing simulation values

Parameter	Value	Uncertainty bound
α	-1.0	N.A.
β	1.0	N.A.
δ	0.2	N.A.
γ	0.1	0.001
ω	1.0	N.A.
x_0	0.1	0.01
$\dot{x}_0$	0.1	0.01
Δt	25.0 s	N.A.

Table 3. 3 DOF simulation values

Parameter	Value	Uncertainty bound
r [m]	3.5145×10^6	50.0
θ [deg]	0.0	0.1
ϕ [deg]	0.0	0.1
v [m/s]	7.032×10^3	1.0
γ [deg]	-15.0	0.1
ψ [deg]	0.0	0.1
ρ_0 [kg/m^3]	0.0158	10^{-5}
w_y[m/s]	N.A.	1.0

The different methods perform well on this simple example. We see that the new approach gives some more conservative bounds and performs better than linear covariance analysis for the same integration step. Note that the black dotted line refers to the 3σ deviation computed using Monte Carlo method (MC), the green line is the 3σ deviation computed by PCE, and the orange line the one obtained through linear covariance analysis. Individual trajectories refers to the sampled trajectories used for Monte Carlo simulation.

3 DOF Entry Vehicle Model

Figure 10 shows the trajectory followed by the center point of the consecutive ellipsoids computed, which follows the shape of the nominal trajectory. Figures 11 to 16 show the uncertainty analysis performance compared to other techniques, the labels match the ones used for the Duffing oscillator. The parameters of the simulation are given in Table 3. The simulation is performed for 80 seconds when the spacecraft basically reaches the proper altitude for potential parachute deployment. Note that Figure 11 and 12 give a concrete example of the safety and conservative nature of the bounds computed using the new method as some sampled trajectories evolve outside of the limits drawn by traditional probabilistic methods.
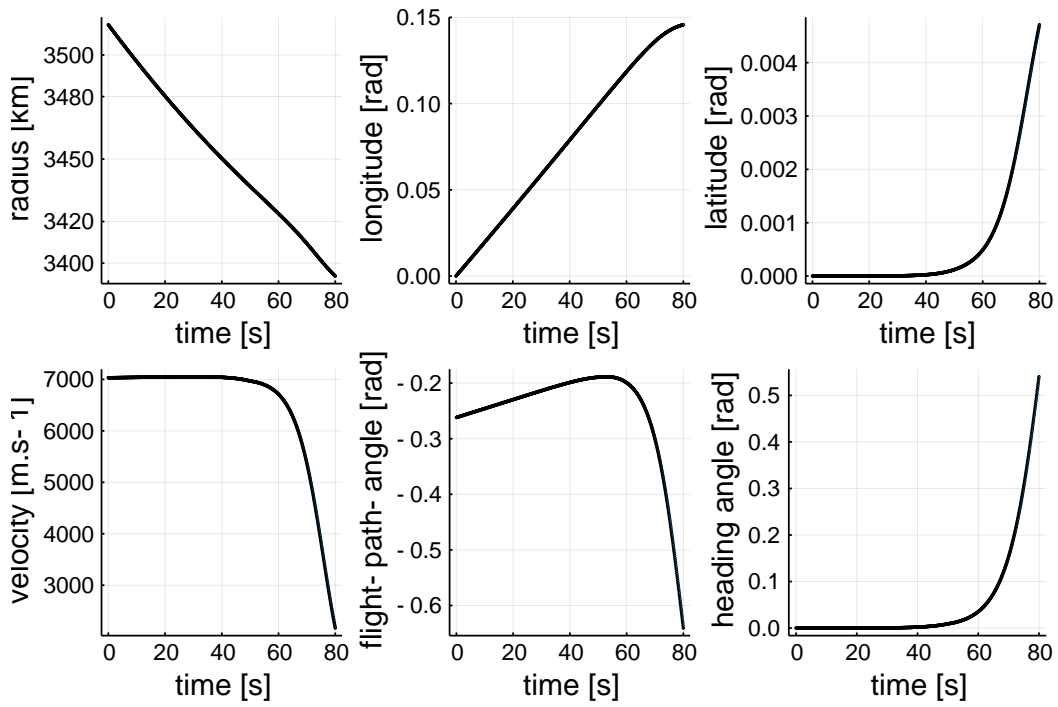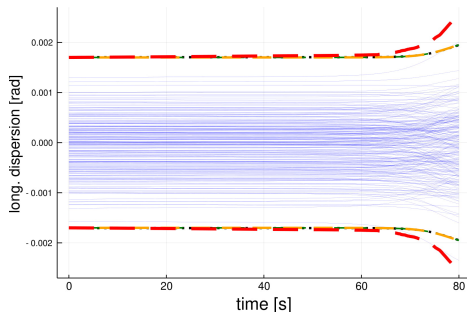
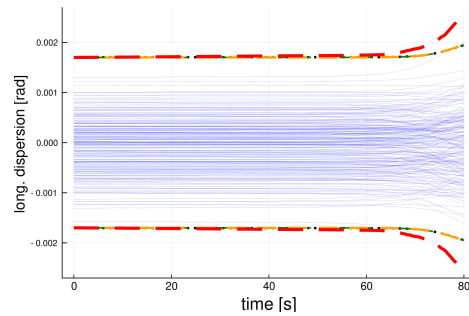**Figure 10. Ellipsoid center trajectory**
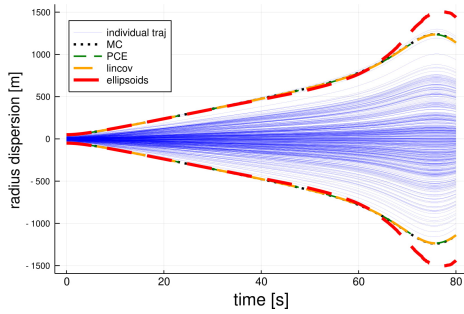
Figure 11. Radius dispersion
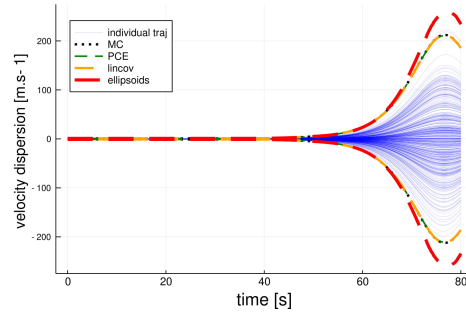
Figure 12. Velocity dispersion

Figure 13. Longitude dispersion
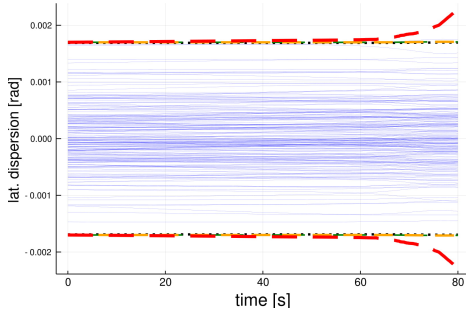

Figure 14. Flight path dispersion
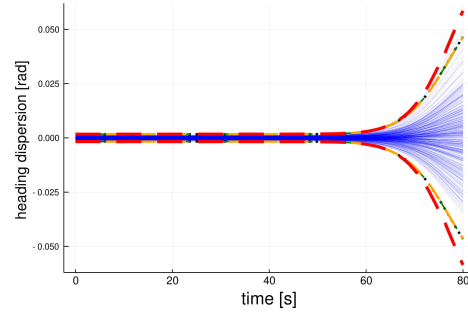
Figure 15. Latitude dispersion

Figure 16. Heading dispersion

6 DOF Entry Vehicle Model

Table 4 summarizes the different parameters used. We have considered uncertainties in the initial state as well as small disturbances in the atmospheric density coefficient and in the relative velocity of the vehicle. The simulation is this time performed during the first phase of entry for approximately 60 seconds.

Table 4. 6 DOF simulation values

Parameter	Value	Uncertainty bound
x [m]	3.5145×10^6	50.0
y [m]	0.0	50.0
z [m]	50.0	1.0
e_x	0.2436	0.005
e_y	-2.09	0.005
e_z	-2.09	0.005
v_x [m/s]	-1.6×10^3	10^{-3}
v_y [m/s]	6.8×10^3	10^{-3}
v_z [m/s]	0.1	10^{-3}
ω_x [rad/s]	0.0	10^{-6}
ω_y [rad/s]	0.0	10^{-6}
ω_z [rad/s]	0.0	10^{-6}
ρ_0 [kg/m^3]	0.0158	10^{-5}
$w_{x,y,z}$[m/s]	N.A.	1.0

Note that the polynomial chaos expansion method has been represented on one of the plots only. An accurate computation using PCE would require a higher order polynomial expansion, not really tractable in a 16-dimensional uncertainty space.

The results of the analysis are shown in Figures 17 to 26. The new approach performs well and always gives conservative bounds on the possible trajectories. While some individual trajectories can evolve outside the 3σ bounds determined by probabilistic-based methods, our conservative method always contain them. It is interesting to realize that linear covariance analysis performs well overall. However if our approach gives relatively high conservative dispersions in position, it clearly stays close to the limits of trajectories and is able to follow the dynamics properly when meeting highly oscillating and non-linear phenomena like it is the case for the attitude of the vehicle.
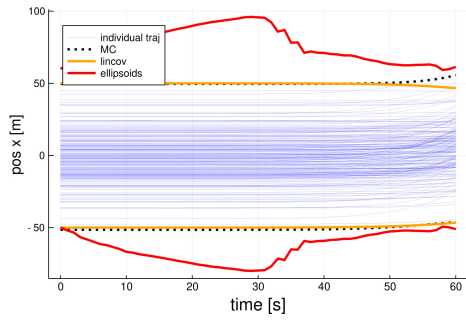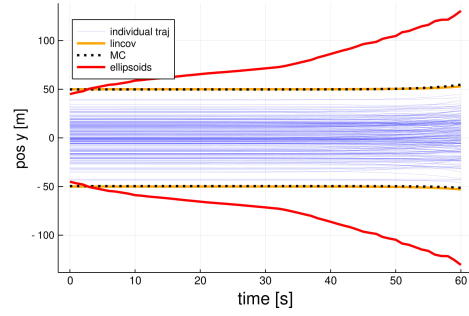
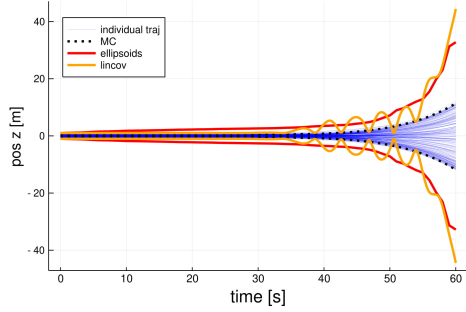**Figure 17. Position x dispersion**

Figure 18. Position y dispersion
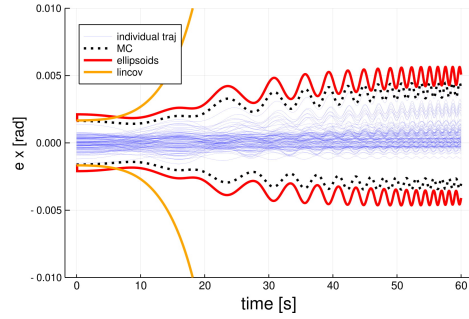

Figure 19. Position z dispersion

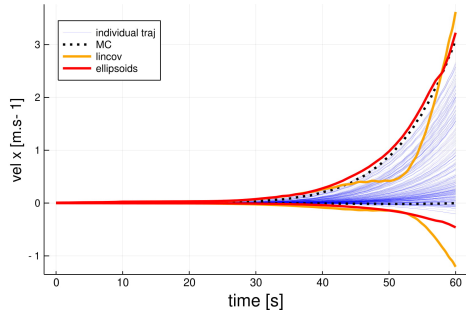**Figure 20. Rotation vector x dispersion**
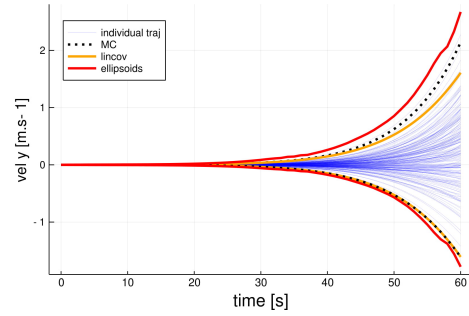

Figure 21. Velocity x dispersion
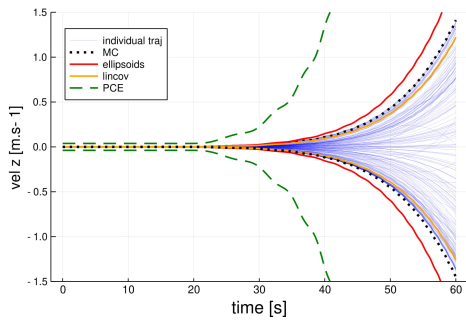

Figure 22. Velocity y dispersion

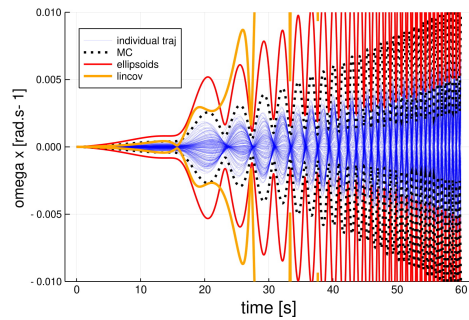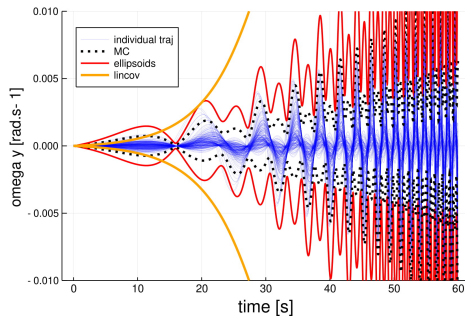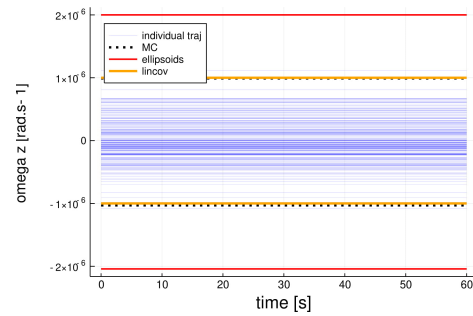**Figure 23. Velocity z dispersion**

Figure 24. Ang. Vel. x dispersion

14

Figure 25. Ang. Vel. y dispersion

Figure 26. Ang. Vel. z dispersion

Linear covariance techniques are dependent on the quality of the linearization techniques which can depend on the system itself. For a given time step, linCov techniques can miss certain non-linearity and predicts tighter bounds like in Figure 21 or too conservative bounds as in Figure 20. Finally the bounds given by MC are usually accurate but do not correspond to conservative limits. In addition, MC is the most computationally heavy technique along with non-intrusive polynomial chaos methods for the 6 DOF analysis.

CONCLUSIONS AND FUTURE WORK

A new uncertainty representation and quantification method for dynamical systems has been introduced. It uses ellipsoidal sets to represent the uncertain regions at each time step and solves a minimum-volume enclosing ellipsoid problem on a chosen set of propagated points, therefore propagating uncertainties in a conservative and safe way. The method has been validated on the Duffing oscillator and then applied respectively to a three and six-degree-of-freedom entry vehicle models, demonstrating the performance of the approach by comparing its application to Monte Carlo, Linear Covariance analysis and Polynomial Chaos Expansion methods.

This approach provides a fast uncertainty quantification method giving conservative bounds on the trajectory, making no assumption on probability distributions followed by the uncertain parameters and is able to take into account the full non-linear dynamics of entry phase. The uncertainty propagation process is differentiable and is therefore well suited for use in optimization procedures (e.g. vehicle design optimization). Future work includes its use in a trajectory optimizer like AL-TRO.[29] At a higher level, the authors are also working on the concrete connection between the sampling scheme and the information propagated during the uncertainty propagation process as well as the deeper link with SOS programming for robust invariant funnels computation.

ACKNOWLEDGEMENT

REFERENCES

[1] R. Prakash, P. D. Burkhart, A. Chen, K. A. Comeaux, C. S. Guernsey, D. M. Kipp, L. V. Lorenzoni, G. F. Mendeck, R. W. Powell, T. P. Rivellini, *et al.*, "Mars Science Laboratory entry, descent, and landing system overview," *2008 IEEE Aerospace Conference*, IEEE, 2008, pp. 1–18.

[2] R. D. Braun and R. M. Manning, "Mars exploration entry, descent and landing challenges," *2006 IEEE Aerospace Conference*, IEEE, 2006, pp. 18–pp.

[3] M. K. Lockwood, R. W. Powell, C. A. Graves, and G. L. Carman, "Entry system design considerations for Mars landers," 2001.

[4] R. D. Braun, R. W. Powell, W. C. Engelund, P. A. Gnoffo, K. J. Weilmuenster, and R. A. Mitcheltree, "Mars Pathfinder six-degree-of-freedom entry analysis," *Journal of Spacecraft and Rockets*, Vol. 32, No. 6, 1995, pp. 993–1000.

[5] D. A. Spencer and R. D. Braun, "Mars Pathfinder atmospheric entry-Trajectory design and dispersion analysis," *Journal of Spacecraft and Rockets*, Vol. 33, No. 5, 1996, pp. 670–676.

[6] A. Prabhakar, J. Fisher, and R. Bhattacharya, "Polynomial chaos-based analysis of probabilistic uncertainty in hypersonic flight dynamics," *Journal of guidance, control, and dynamics*, Vol. 33, No. 1, 2010, pp. 222–234.

[7] K. Jin, D. Geller, and J. Luo, "Development and Validation of Linear Covariance Analysis Tool for Atmospheric Entry," *Journal of Spacecraft and Rockets*, Vol. 56, No. 3, 2018, pp. 854–864.

[8] D. Woffinden, S. Robinson, J. Williams, and Z. R. Putnam, "Linear Covariance Analysis Techniques to Generate Navigation and Sensor Requirements for the Safe and Precise Landing Integrated Capabilities Evolution (SPLICE) Project," *AIAA Scitech 2019 Forum*, 2019, p. 0662.

[9] Y.-z. Luo and Z. Yang, "A review of uncertainty propagation in orbital mechanics," *Progress in Aerospace Sciences*, Vol. 89, 2017, pp. 23–39.

[10] P. S. Maybeck, *Stochastic models, estimation, and control*, Vol. 3. Academic press, 1982.

[11] B. A. Jones, A. Doostan, and G. H. Born, "Nonlinear propagation of orbit uncertainty using non-intrusive polynomial chaos," *Journal of Guidance, Control, and Dynamics*, Vol. 36, No. 2, 2013, pp. 430–444.

[12] D. Xiu, *Numerical methods for stochastic computations*. Princeton university press, 2010.

[13] Z. Manchester and S. Kuindersma, "Robust Direct Trajectory Optimization Using Approximate Invariant Funnels," *Autonomous Robots*, July 2018. pubs-journal, 10.1007/s10514-018-9779-5.

[14] D. Tenne and T. Singh, "The higher order unscented filter," *Proceedings of the 2003 American Control Conference, 2003.*, Vol. 3, IEEE, 2003, pp. 2441–2446.

[15] S. Boyd and L. Vandenberghe, *Convex optimization*. Cambridge university press, 2004.

[16] M. ApS, *MOSEK Optimization Suite. Release 9.1.11.*, 2020.

[17] P. Sun and R. M. Freund, "Summary Conclusions: Computation of Minimum Volume Covering Ellipsoids," 2004.

[18] K. T. Edquist, P. N. Desai, and M. Schoenenberger, "Aerodynamics for Mars Phoenix entry capsule," *Journal of Spacecraft and Rockets*, Vol. 48, No. 5, 2011, pp. 713–726.

[19] T. Zang, A. Dwyer Cianciolo, D. Kinney, A. Howard, G. Chen, M. Ivanov, R. Sostaric, and C. Westhelle, "Overview of the nasa entry, descent and landing systems analysis stud," *AIAA SPACE 2010 Conference & Exposition*, 2010, p. 8649.

[20] M. Grant and R. Braun, "Analytic hypersonic aerodynamics for conceptual design of entry vehicles," *48th AIAA Aerospace Sciences Meeting Including the New Horizons Forum and Aerospace Exposition*, 2010, p. 1212.

[21] A. Bibi, A. Maqsood, and T. H. Go, "Review on Analysis & Modeling of Dynamic Stability Characteristics of Atmospheric Entry Vehicles," *NUST Journal of Engineering Sciences*, Vol. 7, No. 1, 2015, pp. 15–21.

[22] P. Gallais, *Atmospheric re-entry vehicle mechanics*. Springer Science & Business Media, 2007.

[23] J. Benito and K. D. Mease, "Reachable and controllable sets for planetary entry and landing," *Journal of guidance, control, and dynamics*, Vol. 33, No. 3, 2010, pp. 641–654.

[24] J. B. Manrique, *Advances in spacecraft atmospheric entry guidance*. University of California, Irvine, 2010.

[25] N. X. Vinh, A. Busemann, and R. D. Culp, "Hypersonic and planetary entry flight mechanics," *NASA STI/Recon Technical Report A*, Vol. 81, 1980.

[26] F. J. Regan and S. M. Anandakrishnan, *Dynamics of atmospheric re-entry*. American Institute of Aeronautics and Astronautics, 1993.

[27] J. Diebel, "Representing attitude: Euler angles, unit quaternions, and rotation vectors," *Matrix*, Vol. 58, No. 15-16, 2006, pp. 1–35.

[28] F. L. Markley, "Multiplicative vs. additive filtering for spacecraft attitude determination," *Dynamics and Control of Systems and Structures in Space*, No. 467-474, 2004.

[29] T. A. Howell, B. E. Jackson, and Z. Manchester, "ALTRO: A Fast Solver for Constrained Trajectory Optimization," *IEEE/RSJ International Conference on Intelligent Robots and Systems (IROS)*, Macau, China, Nov. 2019. Accepted.